RSC Advances

PAPER

View Article Online
View Journal | View Issue

Check for updates

Cite this: *RSC Adv.*, 2020, **10**, 27225

Preparing 3D-printable silk fibroin hydrogels with robustness by a two-step crosslinking method†

Dafei Gong,[a] Qinrui Lin,[b] Zhengzhong Shao,[b] Xin Chen[b] and Yuhong Yang*[a]

Received 31st May 2020
Accepted 2nd July 2020

DOI: 10.1039/d0ra04789a

rsc.li/rsc-advances

Regenerated silk fibroin (RSF) features excellent biocompatibility and high-strength mechanical properties. However, traditional RSF-based materials can hardly be applied in 3D printing, which has shown great potential in producing artificial implants. In this work, we report a 3D printable RSF hydrogel formed by a weak, chemically crosslinked network. After the 3D printing process, the mechanical properties of the above hydrogel can be remarkably improved by a ripening process. The maximum compressive modulus of this RSF hydrogel is 2.5 MPa, reaching the same order of magnitude as natural elastomers such as cartilage. The mechanical properties of this hydrogel are superior to most RSF-based 3D printed hydrogels. The investigation of gelation mechanism reveals that the chemically crosslinked network can constrain the growth of β-sheet structures of RSF to form a dense and uniform physical network. Such a physically crosslinked network endows the high strength and good resilience of RSF hydrogels. With both good biocompatibility and mechanical properties, this double-network hydrogel has potential in producing 3D printed scaffolds for tissue engineering.

Introduction

3D printing is a technique that directly produces objects in a layer-by-layer manner according to computer-aided design (CAD).[1] In tissue engineering, the features of 3D printing like high automation/repeatability and precise control of microstructures are highly desired for customizing artificial implants for individual patients.[2–5]

Biocompatible and 3D printable hydrogels are usually applied to construct tissue engineering materials.[4] Current 3D printable hydrogels are based on synthetic polymers (such as Pluronic, polyethylene glycol, and poly-*N*-isopropyl acrylamide) and naturally-derived ones (such as gelatin, alginate, chitosan, and silk fibroin).[6] Synthetically-derived hydrogels have advantages in mechanical properties.[7] While the potential toxicity of the degradation products of these hydrogels raises the risks for *in vivo* applications.[7] On the other hand, the hydrogels prepared with naturally derived polymers have been widely utilized to construct tissue engineering materials for the excellent biocompatibility of naturally derived polymers and their degradation products.[8] However, the robustness (usually elastic modulus ranges from 0.01 to 0.1 MPa) of these hydrogels usually does not meet the requirements for artificial cartilage (elastic modulus about 1 MPa).[9,10]

Regenerated silk fibroin (RSF) based hydrogels are ideal materials in tissue engineering for properties like being processed in water phase, low immunogenicity, and excellent mechanical properties.[11] Robust RSF hydrogels can be formed through physical or chemical interactions.[11,12] However, these RSF-based hydrogels can hardly be 3D printable because the β-sheet network can clog in the needles.[5,13] Current 3D printable RSF-based hydrogels are realized by mixing RSF with other printable polymers, such as gelatin,[14] collagen,[15] decellularization matrix,[16] and hydroxypropyl methyl cellulose.[17,18] Although the additive polymers made RSF 3D printable, these hydrogels cannot retain the outstanding mechanical properties of RSF hydrogels.

In this paper, we tried to solve the 3D printable problem of RSF-based hydrogels by preparing a weak and chemically crosslinked network. This weak hydrogel did not clog in the needles during printing process and can maintain the designed structures after being printed. After 3D printing, the physically crosslinked network was formed by treating chemically crosslinked hydrogel with ethanol so that the compressive modulus of this RSF hydrogel can be elevated to 2.5 MPa. The origin of such outstanding mechanical properties was further investigated by Raman spectroscopy, ^{13}C CP-MAS NMR and light transmittance experiments. In addition, *in vitro* cytotoxicity and preliminary cell culture experiments had demonstrated that this hydrogel is biocompatible in cell culture.

Experimental

Materials

Silkworm cocoons were purchased from farmers in Nantong; carbic anhydride, Irgacure 2959 (I2959), and dithiothreitol

[a]*Research Center for Analysis and Measurement, Fudan University, 220 Handan Road, Shanghai 200433, People's Republic of China. E-mail: yuhongyang@fudan.edu.cn*

[b]*Department of Macromolecular Science, Laboratory of Advanced Materials, Fudan University, 220 Handan Road, Shanghai, 200433, People's Republic of China*

† Electronic supplementary information (ESI) available. See DOI: 10.1039/d0ra04789a

(DTT) were purchased from Aladdin Reagent Co., Ltd.; Na_2CO_3, LiBr, H_3BO_3, $Na_2B_4O_7$, NaOH, PEG ($M_n = 20\,000$), ethanol were purchased from Sinopharm Chemical Reagent Co., Ltd.

Preparation of RSF aqueous solution

The aqueous solution of RSF was prepared according to an existing method.[19] In order to remove sericin, the cocoons were boiled in a 0.5 wt% Na_2CO_3 solution at 100 °C for 40 min, washed with deionized water and dried to obtain degummed silk fibroin. Then degummed silk fibroin was dissolved in a 9.3 M LiBr solution at 40 °C for 40 min. After removing insoluble impurities by filtration, the RSF solution was dialyzed in deionized water for 3 days to remove LiBr (the molecular weight cut off is 14 000 Da). After dialysis, the solution was centrifuged at 8000 rpm for 8 min and the supernatant was stored in a refrigerator at 4 °C. The concentration of this RSF solution was measured by weight method.

Functionalization of RSF solution with norbornene

Norbornene was conjugated to silk fibroin molecules according to a previous report.[20] The RSF solution was diluted to 1 wt% with a boric acid-borax buffer (pH = 9.0) and carbic anhydride was subsequently added to above RSF solution with 5 wt% in concentration. The reaction was kept in dark and gently stirred at room temperature for 24 h. 2 M NaOH was used to maintain at a pH of 8–9 during the reaction. After the reaction was completed, the norbornene modified RSF (RSF-NB) solution was filtered, dialyzed in deionized water for 3 days and concentrated by reverse dialysis with a PEG ($M_n = 20\,000$) aqueous solution to reach a concentration about 20 wt%.

Preparation of double-network RSF hydrogel

The preparation of the double-network RSF hydrogel was a two-step process. First, DTT and I2959 were dissolved in deionized water at 60 °C and cooled to room temperature.[21] RSF-NB solution was mixed with above solution at different concentrations of I2959 (0.05–0.5 wt%), DTT (mass ratio DTT : RSF-NB 1 : 200–1 : 5), RSF-NB (5–15 wt%) to obtain precursor solutions. The precursor solutions were irradiated under a hand-held ultraviolet lamp (365 nm) to obtain chemically cross-linked RSF hydrogels. The distance between the samples and the light source was kept around 25 mm. The obtained hydrogels were soaked in ethanol for at least 24 h, and then immersed in deionized water for three days to obtain double-network RSF hydrogels.

NMR

^{1}H NMR test. ^{1}H NMR test was performed on an Avance III HD liquid NMR spectrometer (Bruker, Germany) with a resonance frequency of 500 MHz. The sample preparation process was as follows: a 15 wt% RSF solution, a 15 wt% RSF-NB solution, and a 15 wt% chemically crosslinked RSF hydrogel were froze in liquid nitrogen, freeze-dried and ground into powder. The obtained powders and carbic anhydride were separately dissolved in deuterated trifluoroacetic acid at a concentration of 1 wt% (the lyophilized powder of the chemically crosslinked RSF hydrogel was dissolved for two weeks). The ^{1}H NMR test used a 90° pulse train with a delay time of 6 s, a pulse intensity of 11.5 μs, a pulse width of 11.46 dB, a spectral width of 20 ppm, and a scan count of 128 times. The test was done at room temperature.

^{13}C CP-MAS NMR test. The ^{13}C CP-MAS NMR test was performed on an Avance III solid-state nuclear magnetic resonance spectrometer (Bruker, Germany) with a resonance frequency of 100 MHz. The preparation process of the powder samples remained the same with that for ^{1}H NMR test. Test conditions: cross-polarization time 2 ms, delay time 3 s, scan accumulation times 800, pulse width 5 μs, ^{1}H decoupling frequency 50 kHz, 4 mm probe, 10 kHz. Chemical shifts were calibrated using carbon at 17.3 ppm on hexamethylbenzene. Since the C_β peak (12–28 ppm) on the alanine residue in silk fibroin is sensitive to the silk I and silk II structures of silk fibroin, this peak was deconvoluted by Gaussian fitting to evaluate both the content of the structures under different conditions.

Rheology test

Rheology performance tests were performed on a Physica MCR Model 301 rheometer (Anton Paar GmbH, Austria) using 25 mm diameter parallel plates. The dynamic viscoelasticity of the chemically crosslinked RSF hydrogel was tested at frequency 1 Hz, the test temperature was set at 25 °C, the normal force was 0 N, and the strain amplitude scanning from 0.1% to 100% was performed. The shear-thinning test was recorded at frequency 1 Hz. During the destruction and recovery stage, the large strain amplitude of 1000% and the small strain amplitude of 1% (which is within the linear viscoelastic regime) were selected. In order to reduce the impact of hydrogel drying on the test results, an anti-volatile mask was used throughout the test.

Mechanical properties

The mechanical properties of the hydrogels were tested on an Instron 5565 electronic universal material testing machine (Instron, UK) with a 500 N sensor at room temperature. For uniaxial compression test, the hydrogel samples were molded into a cylinder with 12 mm in width and 10 mm in height. The compression strain was set to 30% in the cyclic compression test and the compression rate was 100%/min. The number of cyclic compressions was 10, and the compression interval was 1 min. For the tensile tests, hydrogels were made into a dumb-bell shape with 4 mm in width, and about 2 mm in thickness. The gauge length was 15 mm and the elongation rate was 10 mm min^{-1}. For each measurement, five hydrogel samples were tested.

Raman spectroscopy

Raman spectroscopy was performed on an XploRA laser Raman spectrometer (HORIBA, France). The samples were prepared in the same process as that for ^{13}C CP-MAS NMR experiments. The Raman spectra were obtained with grating of 1200, excitation wavelength of 785 nm, laser power of 90 mW, 10 s accumulation and 10 times scan.

Light transmittance experiments

The light transmittance tests were performed on a UV Model 2910 UV-Vis spectrophotometer (Hitachi, Japan), with 300 to 800 nm in wavelength range and 400 nm min^{-1} in scanning speed. All hydrogels were 15 wt% in solid content and *in situ* formed in a 5 mm cuvette.

3D printing of hydrogel

The hydrogels were 3D printed with a Bio-Architect®-WS biological 3D printer (Regenovo, China). The hydrogels were prepared as follows: firstly, the precursor solutions were prepared with 0.5 wt% of I2959, DTT and RSF-NB mass ratio of 1 : 50, and 15 wt% concentration of RSF-NB and irradiated at 365 nm wavelength ultraviolet light for 2–5 min. The obtained solutions were immediately transferred to the barrel and matured for at least 1 h. The chemically crosslinked hydrogels were extruded by air pressure using a conical needle with a diameter of 400 μm. The printing process set the air pressure to 0.15–0.3 MPa and the printing speed to 3–7 mm s^{-1}.

In vitro cytotoxicity evaluation

The double-network RSF hydrogels were sterilized by 75% ethanol and then immersed in a sterilized PBS buffer to remove ethanol. The double-network hydrogels were extracted in a serum-free DMEM medium for 24 h at 37 °C. Mouse fibroblast (L929) cells were seeded in a 96-well plate with 1×10^4 cells per well. The seeded L929 cells were co-incubated with the extracts in different concentrations (25%, 50%, 75%, 100%). After 24 h and 72 h, cell viability was tested by CCK-8 kit.

Cell culture

The hydrogels were sterilized with the same method for cytotoxicity experiments. L929 cells were seeded onto the double-network hydrogels with 10^6 in density and cultured for 72 h. Then, the cells were stained with a Live/Dead assay (*i.e.*, fluorescein oxalic acid and propidium iodide), and observed using an IX fluorescence microscope (Olympus, Japan). A C^{2+} type laser scanning confocal microscope (Nikon, Japan) was used to observe cell distribution in hydrogels.

Results and discussion

Fabrication and characterization of the chemically crosslinked RSF hydrogels

The chemically crosslinked network was prepared using norbornene modified RSF molecules and DTT. The amino groups in silk fibroin were utilized to conjugate with carbic anhydride. Since these amino groups of lysine and arginine residues are located on hydrophilic segment of the heavy chain,[22] carbic anhydride and silk fibroin can react in mild and aqueous conditions. Moreover, amino groups do not involve the formation of β-sheet. This modification process will not inhibit β-sheet formation in the following ethanol treatment. In comparison with pure RSF (red line in Fig. 1A), the NMR spectrum of RSF-NB presents a new chemical shift at 6.4 ppm (green line in Fig. 1A), which is attributed to the hydrogen on C=C of carbic anhydride (ESI Fig. S1A†). This result indicates that norbornene functional group was successfully modified on the silk fibroin.

Then, the feasibility of this RSF-NB precursor for chemical crosslinking was investigated with DTT as the crosslinker and I2959 as the photoinitiator. After being irradiated for one hour at 365 nm, the RSF-NB precursor with RSF-NB concentration of 10 wt% was converted into translucent, self-supporting chemically crosslinked RSF hydrogel (ESI Fig. S2†). Also, the viscosity and the storage modulus of the RSF-NB precursor increased by three orders of magnitude, and the loss factor decreased from 0.66 to 0.08 (Fig. 1B and ESI Fig. S3†). Such variation in viscosity and storage modulus further confirmed that the norbornene functionalized silk fibroin can be chemically crosslinked.

This sol–gel transition was further studied using NMR on molecular level. After irradiating the hydrogel with UV light, the chemical shift at 6.4 ppm of RSF-NB disappeared (blue line in Fig. 1A). This phenomenon indicates that the UV irradiation induces the reaction between the C=C group of norbornene and the thiol group of DTT. Since the chemically crosslinked hydrogel can be degraded by trifluoroacetic acid during sample preparation for NMR, the impact of sample preparation on C=C bond was also studied using carbic anhydride treated by trifluoroacetic acid for 14 d. The chemical shift at 6.4 ppm on the NMR spectrum of trifluoroacetic acid treated carbic anhydride remains the same with that of norbornene (ESI Fig. S1B†). Thus the chemical shift of C=C bond is not impacted by sample preparation and this sol–gel transition is attributed to chemical reaction between norbornene and thiol groups. According to the literature, the degree of thiol–ene click reaction can be controlled by irradiation conditions (such as laser power and irradiation time).[23] This chemically crosslinked RSF hydrogel has tunable degree of crosslinking, which is advantageous for preparing 3D printable RSF hydrogels.

To improve the mechanical properties of chemically crosslinked hydrogels for tissue engineering, the feeding ratio of reactive agents and the solid content of the chemically crosslinked RSF hydrogel were further optimized.

The mechanical properties of chemically crosslinked hydrogels with different solid contents of RSF-NB were firstly investigated by dynamic rheology. As concentration of RSF-NB increased from 5 wt% to 15 wt%, the storage modulus of chemically crosslinked RSF hydrogels increased significantly from 19 Pa to 1.1 kPa (Fig. 2A). Although the light transmittance of the precursor solutions reduced slightly when RSF-NB concentration increased (ESI Fig. S4†), the storage modulus of the hydrogel with 15 wt% in solid content was much higher than that with 10 wt%. Further increase in solid content is not practical because RSF-NB tends to gelate during concentrating. Therefore, the concentration of the RSF-NB in this study was fixed to 15 wt%.

Then the feeding ratio of the crosslinker DTT was optimized to improve the mechanical properties.[24] When the mass ratio of DTT to RSF-NB increased from 1 : 200 to 1 : 50, the storage modulus of chemically crosslinked hydrogel gradually increased from 77 Pa to 1.1 kPa, and the loss factor decreased

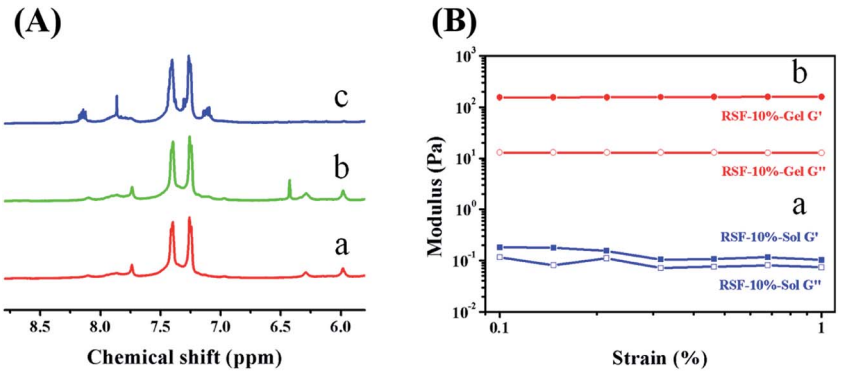

Fig. 1 (A) Enlarged ^{1}H NMR spectra of (a) RSF, (b) RSF-NB and (c) chemically crosslinked RSF. (B) Viscoelastic properties of 10 wt% RSF-NB aqueous solution and 10 wt% chemically crosslinked RSF hydrogel.

from 0.15 to 0.05 (Fig. 2B). When the mass ratio further increased from 1 : 50 to 1 : 10, the storage modulus of the hydrogel gradually decreased from 1.1 kPa to 0.9 Pa, and the loss factor increased from 0.05 to 1.89. In the end, the hydrogel was not self-supporting. This variation can be explained as follows: when the amount of DTT is insufficient, RSF-NB is not fully reacted; as the content of DTT increases, the degree of reaction gradually increases so that the mechanical properties of hydrogels also increase; when DTT is excess, additional DTT will block of the reactive sites on RSF-NB so that decreasing in storage modulus observed. Thus, the mass ratio of DTT to RSF-NB of 1 : 50 was chosen for preparing chemically crosslinked RSF hydrogels.

In addition, the effect of the amount of photoinitiator added was also investigated in this study. I2959 is a slightly water-soluble and cytotoxic photoinitiator. It has been reported that it shows obvious cytotoxicity if the concentration of I2959 is more than 0.1 wt%.[25] In this work, the residual I2959 can be removed in the curing and sterilization of the hydrogel.[26] Therefore the amount of I2959 can be optimized without concerning its cytotoxicity. For 1 h irradiation, when the amount of I2959 increased from 0.05 wt% to 0.5 wt%, the storage modulus

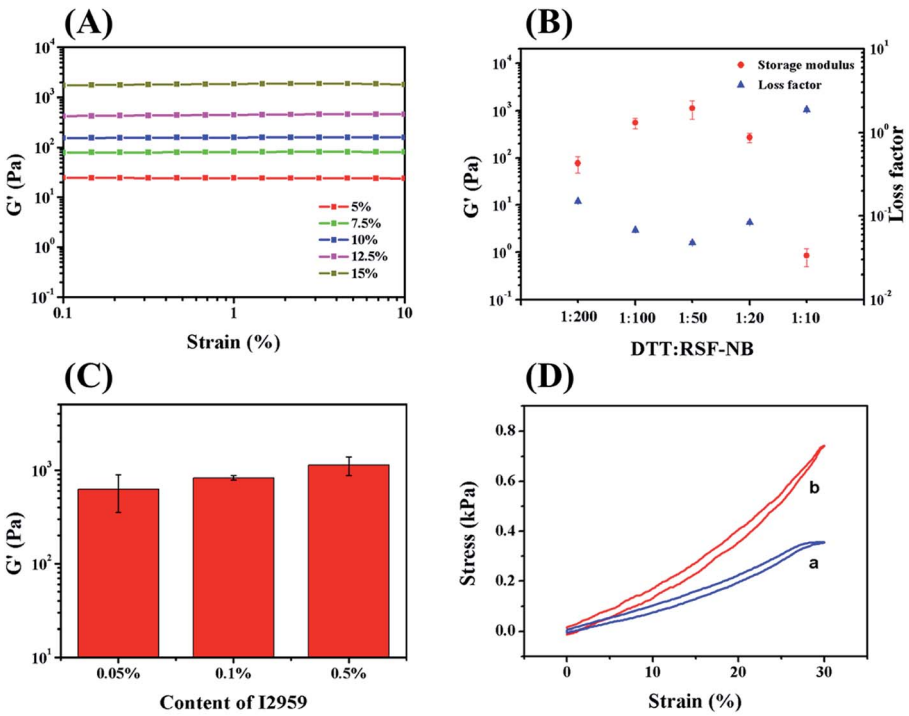

Fig. 2 (A) Representative storage modulus *versus* strain for chemically crosslinked RSF hydrogels with different RSF-NB solid contents (DTT : RSF-NB = 1 : 50). (B) The effect of DTT/RSF-NB mixing ratio on the viscoelastic properties of chemically crosslinked RSF hydrogels. (C) The effect of content of I2959 on the viscoelastic properties of chemically crosslinked RSF hydrogels. (D) The representative compression hysteresis cycles of chemically crosslinked hydrogels. (a) 12.5 wt%, (b) 15 wt%. These chemically crosslinked RSF hydrogels were all irradiated for 1 h and then measured.

of the chemically crosslinked hydrogel increased from 0.6 kPa to 1.1 kPa (Fig. 2C). This variation was attributed to the sufficient radicals provided by sufficient of photoinitiator to crosslink RSF-NB and DTT. Since I2959 tended to precipitate in higher concentration, therefore, 0.5 wt% of I2959 was chosen for preparing chemically crosslinked RSF hydrogels. After optimization of experimental conditions, as-prepared chemically crosslinked hydrogels exhibit small hysteresis loops and good resilience (Fig. 2D), with 1.2 kPa (12.5 wt%) and 1.8 kPa (15 wt%) in compressive modulus, respectively. According to previous reports, such storage modulus is suitable for extrusion based 3D printing.[27]

Furthermore the feasibility of above hydrogel for 3D printing was evaluated by shear-thinning test using 10 wt% hydrogel as an example. The chemically crosslinked hydrogel exhibits shear-thinning behaviors which ensure the hydrogel not clogging in the needles during printing. Although the storage modulus of this hydrogel decreased to 70 Pa after structural destruction, the gel-like rheological properties of the chemically crosslinked hydrogel still remain with its storage modulus much over loss modulus (ESI Fig. S5†). Therefore, the hydrogel can hold its shape during and after 3D printing. Above shear-thinning behaviors as well as the image of a printed scaffold with the chemically crosslinked hydrogel confirm that RSF molecules can be 3D printable by preparing a weak, chemically crosslinked RSF hydrogel (ESI Fig. S6†).

Mechanical properties of double-network RSF hydrogels

In order to improve the mechanical properties of the chemically crosslinked RSF hydrogels, ethanol was utilized to physically crosslink the hydrogel by inducing the formation of β-sheet structure of RSF. Also, this process can remove the cytotoxic I2959. After being treated with ethanol, the translucent chemically crosslinked hydrogel (ESI Fig. S7A†) became white and opaque because of increase in β-sheet structure (ESI Fig. S7B†). This double-network hydrogel, consisting of chemically crosslinked and physically crosslinked networks, exhibited excellent strength and flexibility so that it can withstand the weight of 735 times of its own (Fig. 3A) and maintain its shape when bent nearly 180° in a repeated bending test (Fig. 3B).

The mechanical properties of this double-network RSF hydrogel were also evaluated by compression (Fig. 4) and tensile experiments. The compressive modulus after ethanol treatment increased by three orders of magnitude (Table 1) and up to that of natural cartilages. The compressive modulus of 15 wt% group increased from 1.8 kPa to 2.5 MPa, such variation is similar to that of the chemically crosslinked hydrogels. In the multi-cycle compression test, the compressive modulus of these hydrogels has decreased significantly after the first cycle. Therefore the double-network hydrogel may undergo partial plastic deformation at 30% compressive strain. In the subsequent multiple cycles, the hysteresis loops are reduced and the double-network hydrogels exhibit good resilience like elastomers. Besides, the Young's modulus of 10 wt% double-network RSF hydrogel was similar to its compressive modulus, which exceeded 1.0 MPa (ESI Fig. S8†). Therefore, this double-network hydrogel can be used as artificial implants because it has similar mechanical properties with natural cartilages.

Investigation of the gelation mechanism of the robust double-network RSF hydrogel

After treating the chemically crosslinked hydrogel with ethanol, the compressive modulus of the RSF hydrogel increased more than 1000 times, which is significantly higher than that of natural RSF hydrogel induced by ethanol. Therefore, the physically and chemically crosslinked networks have synergetic contributions to the mechanical properties of the double-network hydrogel. Raman, NMR, and UV-Vis spectroscopy were utilized to further investigate the contributions of these two networks in the hydrogel.

Before chemical crosslinking, the Raman spectra of pure RSF, RSF-NB and the precursor solution have a broad scattering peak around 1660 cm^{-1}. These solutions were dominated by random coil structures and small amount of other secondary structures (Fig. 5A, line a, b and c).[28] Also in the Raman spectrum of the precursor solution, the broad amide III band (around 1250 cm^{-1}) revealed that the random coils are the dominant structures and the modification of norbornene groups as well as DTT and I2959 has negligible impact on the secondary structure of silk fibroin.[28] After chemical

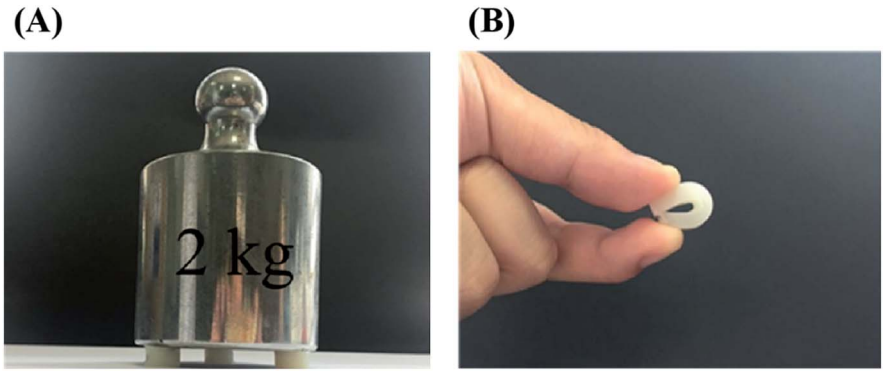

Fig. 3 (A) 2 kg of weights were placed on three RSF hydrogels, each hydrogel was about 12 mm in diameter and 10 mm in height. (B) Bent nearly 180 degrees. All hydrogels in this figure are in solid content of 15 wt%.

crosslinking, a sharp peak attributed to β-sheet appeared at 1667 cm^{-1} (Fig. 5A, line d). This transition indicates that chemical crosslinking not only crosslinks the lysine and arginine residues in the silk fibroin molecules, but also induces the conformational transition of protein from random coil to β-sheet.[29] After ethanol treatment, the amide I band of the double-network hydrogel is sharper (Fig. 5A, line e), indicating that the content of β-sheet structure in the hydrogel further increased and structure was perfected.

Then ^{13}C CP/MAS NMR spectroscopy was applied to estimate the variation of the content of β-sheet structure in the preparation of the double-network RSF hydrogel. In the ^{13}C CP/MAS NMR spectrum of RSF, the chemical shift around 12 to 28 ppm is attributed to C_β on the alanine residue of silk fibroin and very sensitive to the variation of secondary structures in silk fibroin. According to the literature, C_β can be divided into three components. The chemical shift at 16.7 ppm is attributed to the random coil and twisted β-turn structures. The chemical shifts at 20.0 ppm and 22.4 ppm are attributed to the methyl groups on alanine residues of β-sheet structures. These two methyl groups are in two different directions: perpendicular and parallel to the β-sheet structures, respectively.[30] The fractions of above three chemical shifts and their proportions in the whole C_β region can be used to estimate the contents of different secondary structures.

Random coil and β-turn structures are the dominant structures in RSF, RSF-NB and precursor solutions (ESI Fig. S9†). As shown in Table 2, the contents of β-sheet structure are similar in above solutions (19.8%, 21.9%, and 23.0%, respectively). These data revealed that the conformation of the silk fibroin molecules before the chemical crosslinking did not change significantly. After thiol–ene reaction, the content of β-sheet structure of chemically crosslinked RSF hydrogel increased from 23.0% to 30.7%, which is consistent with that

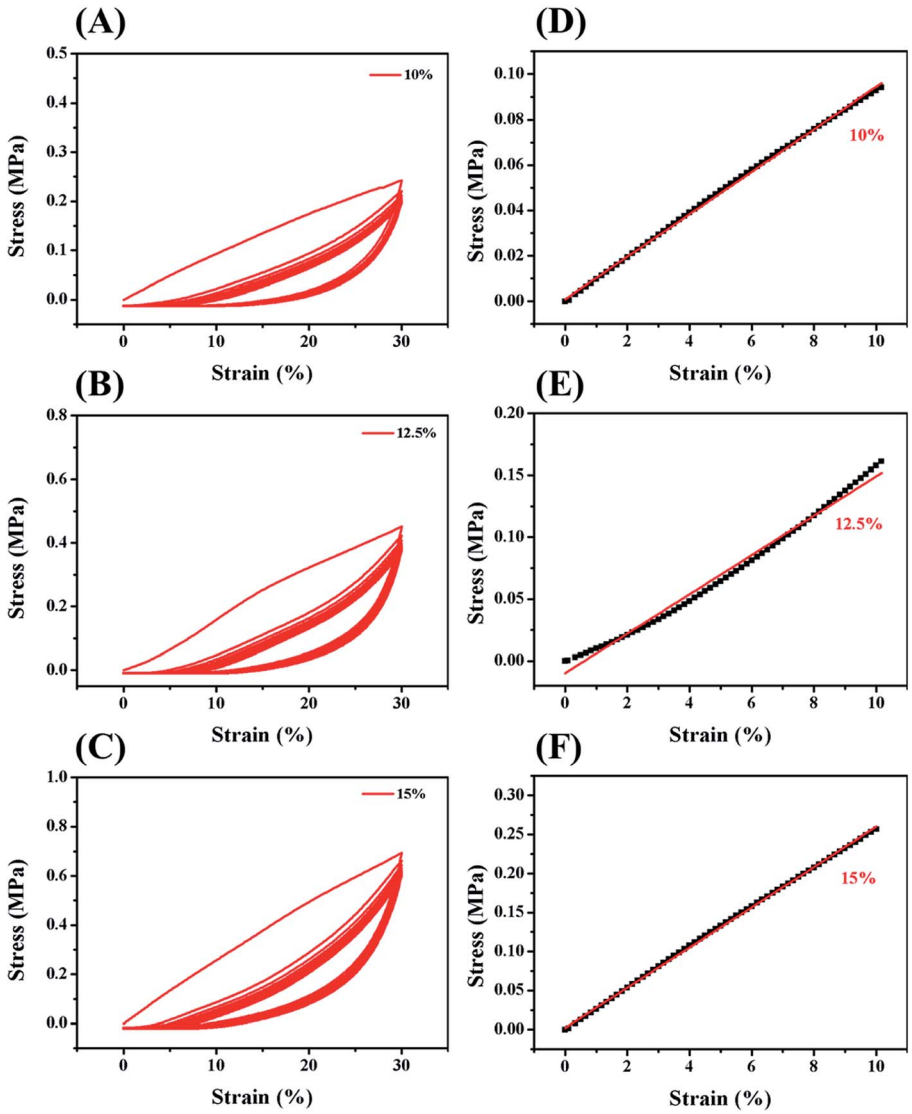

Fig. 4 Representative stress–strain curves of cyclic compressive test of double-network RSF hydrogels of (A) 10 wt%, (B) 12.5 wt%, (C) 15 wt%. Representative linear fittings of double-network RSF hydrogels with different solid contents, (D) 10 wt%, (E) 12.5 wt%, (F) 15 wt%.

Table 1 Compressive modulus of chemically crosslinked RSF hydrogels and double-network RSF hydrogels with different solid contents

Solid content	Chemically crosslinked hydrogels	Double-network hydrogels
10 wt%	ND	0.9 ± 0.0 MPa
12.5 wt%	1.2 ± 0.2 kPa	1.4 ± 0.2 MPa
15 wt%	1.8 ± 0.3 kPa	2.5 ± 0.3 MPa

characterized by Raman spectroscopy. Therefore, irradiating with 365 nm light can induce structure transition of RSF molecular chains. After ethanol treatment, the content of β-sheet structure of the double-network RSF hydrogel increased significantly to 60.4%, which is close to that of the RSF hydrogel formed by natural aggregation. However, the mechanical properties of the double-network hydrogel are significantly better than those of naturally aggregated hydrogels. This phenomenon cannot be fully explained by the increase of the content of β-sheet structure.

In addition to the content of β-sheet structure, size and size distribution of β-sheet structures are also contributed to the mechanical properties of RSF hydrogels.[12,31] These two parameters can be estimated by the transmittance of RSF hydrogels. In visible light region (400–700 nm), the light transmittance of the chemically crosslinked RSF hydrogel remains above 90% (Fig. 5B, line a). While the content of β-sheet structure in this hydrogel is about 30% according to ^{13}C NMR spectroscopy. The phenomenon can be attributed to imperfect β-sheet structure in RSF and negligible density variation in this hydrogel, which is also confirmed by compression experiments (Fig. 2D). In contrast, a decrease of transmittance was observed in the case of the double-network hydrogel. However, it still exhibited much higher transmittance in comparison with naturally cured RSF hydrogels and hydrogels formed by ethanol within the visible range (Fig. 5B, line b, c and d). This means that the size of β-sheet structure in the double-network hydrogel is much smaller than that of the other two RSF hydrogels. Since these three hydrogels have similar contents of β-sheet structure, the smaller of the size of β-sheet structure, the more uniform of the size distribution of β-sheet structure in RSF hydrogel. Normally, β-sheet structures serve as the physically crosslinked points in RSF hydrogel, it is reasonable to speculate that the content and distribution uniformity of physical crosslinker are much higher in the double-network hydrogel than that in the other two hydrogels, so that the mechanical properties of the double-network hydrogel can be significantly improved.

Based on the above characterizations of mechanical properties and secondary structures, the formation of the robust RSF hydrogel was supposed as follows: (1) in the chemical crosslinking process, random coil structures in the silk fibroin molecules were partly destructed so that the silk fibroin molecules were loose and the possibilities for inter-chain reactions

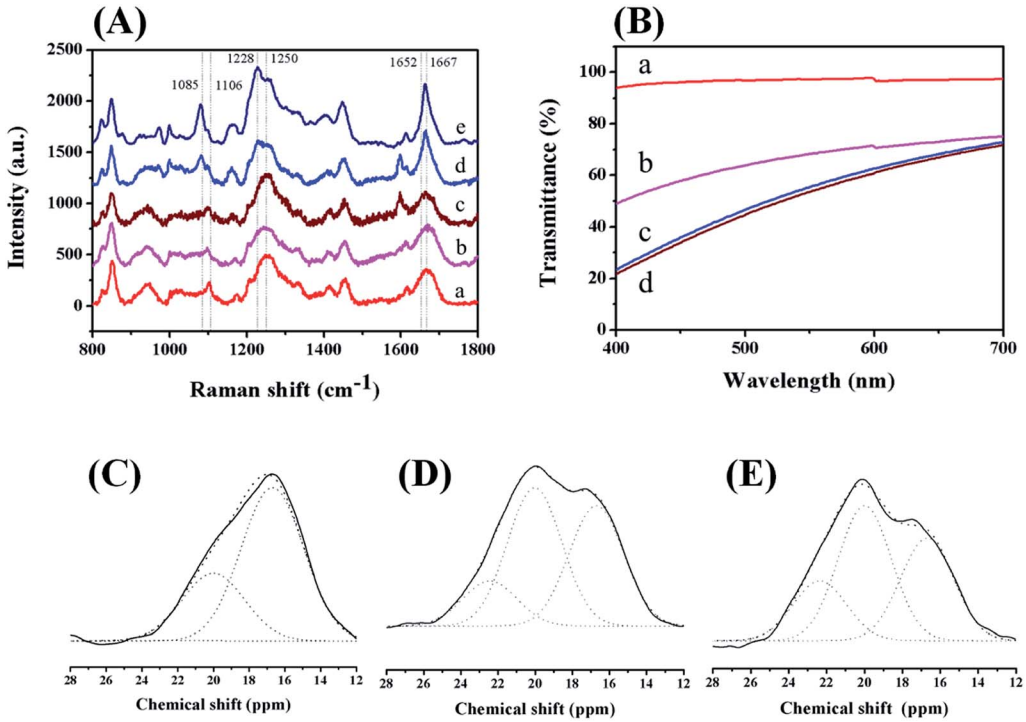

Fig. 5 (A) Raman spectra of freeze-dried samples of (a) RSF solution, (b) RSF-NB solution, (c) precursor solution, (d) chemically crosslinked RSF hydrogel, (e) double-network RSF hydrogel. (B) Transmittance spectra of (a) chemically crosslinked RSF hydrogel, (b) double-network RSF hydrogel, (c) naturally formed RSF hydrogel and (d) naturally formed RSF hydrogel after ethanol treatment with a thickness around 1.18 mm in RSF solid content of 15 wt%. ^{13}C NMR spectra and simulated ones of (C) chemically crosslinked RSF hydrogel, (D) double-network RSF hydrogel and (E) naturally formed RSF hydrogel.

Table 2 Fractions of secondary structures in freeze-dried RSF samples

Samples	Fractions of peak at 16.7 ppm	Fractions of peak at 20.0 ppm	Fractions of peak at 22.4 ppm
RSF solution	80.2%	19.8%	0
RSF-NB solution	78.1%	21.9%	0
Precursor solution	77.0%	23.0%	0
Chemically crosslinked hydrogel	69.3%	30.5%	0.2%
Double-network hydrogel	39.6%	45.5%	14.9%
Naturally formed hydrogel	34.5%	45.4%	20.1%

increased; (2) during ethanol treatment, the chemical network constrained the growth of the β-sheet structure resulting to a small and uniform distribution of β-sheet structure in the whole hydrogel.

Feasibility of the 3D printed double-network RSF hydrogel for cell culture

Hydrogel for tissue engineering should be biocompatible. Therefore, the biocompatibility of the double-network hydrogel was firstly investigated by testing the cytotoxicity of L929 fibroblasts incubated with the hydrogel extracts. Assayed by CCK-8, the cell viabilities of different diluted extracts were all above 95% (Fig. 6A). Considering cells cannot grow normally on the chemically crosslinked hydrogel (ESI Fig. S10†), the treatment of ethanol also works for removing the cytotoxic DTT and I2959. Therefore, the double-network hydrogel maintains the biocompatibility of protein-based materials and can be further applied in tissue engineering.

Hydrogels for 3D printing should possess suitable rheological properties.[27] The double-network hydrogels with high strength cannot be printed because they would jam in the needle. Since the modulus of the chemically crosslinked hydrogel can be controlled by the degree of crosslinking,[23] the rheological properties of the hydrogel can be manipulated by varying irradiation time. When being irradiated for 3 min at 365 nm, the precursor solution with 15 wt% RSF-NB was still fluid. One hour after the irradiation by UV light, the precursor solution turned into a translucent and self-supporting hydrogel. It means that the thiol–ene reaction still continued without UV

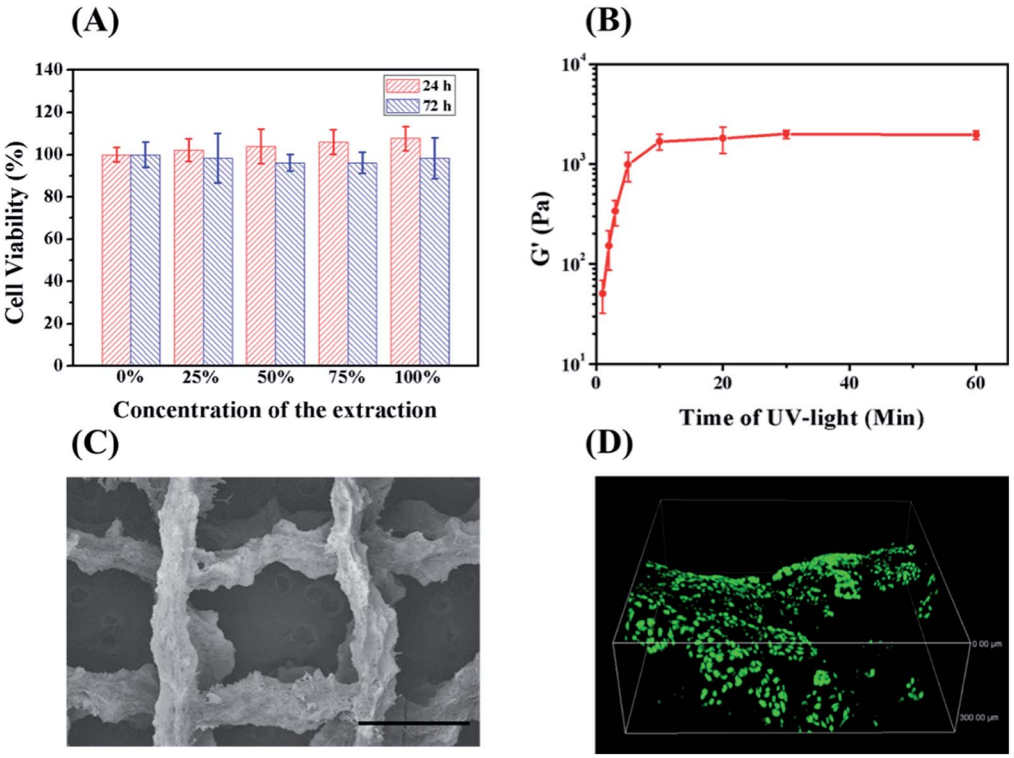

Fig. 6 (A) *In vitro* cytotoxicity of L929 cells cultured with double-network hydrogel extractions of different concentrations for 24 h and 72 h. (B) Storage moduli of chemically crosslinked RSF hydrogels *versus* irradiation time of UV-light. All chemically crosslinked RSF hydrogels were measured after removing the ultraviolet light for 1 h. (C) SEM image of freeze-dried 3D printed double-network RSF hydrogel. Scale bar is 1 mm. (D) Confocal laser scanning microscopy (CLSM) image of L929 cells incubated in 3D printed double-network RSF hydrogel for 3 days.

light due to the presence of residual radicals.[32] The viscoelasticity of above hydrogels along irradiation time was further investigated. Fig. 6B is the plot of the ultimate storage modulus of the chemically crosslinked hydrogels *versus* irradiation time of UV light. The ultimate storage modulus increased from 51 Pa to 1.7 kPa as the UV exposure time increased from 1 min to 10 min. When the UV exposure time exceeded 10 min, the storage modulus of the hydrogel almost changed no more. For 3D printing, if the irradiation time is too short, the chemically crosslinked RSF hydrogel will be too weak to maintain its shape during 3D printing. If the irradiation time is too long, the chemically crosslinked RSF hydrogels tend to clog in the needle. Therefore, the irradiation time was chosen to be 2 to 5 min to prepare a 3D-printable hydrogel. Based on the previous study on the mechanical properties and formation mechanism of hydrogels, after 3D printing of chemically crosslinked hydrogels, ethanol was applied to improve the mechanical properties of the hydrogel as well as remove cytotoxic residuals (Fig. 6C is an SEM image of a lyophilized stent of a 3D printed double-network RSF hydrogel).

To investigate the feasibility of 3D printed double-network RSF hydrogels for tissue engineering, L929 cells were further seeded on the hydrogel scaffold. After 3 days, L929 cells were stained by Live/Dead assay. Dead cells (with red emission) were hardly observed in the hydrogel scaffold while live cells (with bright green emission) were observed in the view (ESI Fig. S11†). Confocal microscopy was further adopted to investigate the state of seeded cells in 3D. L929 cells were well spread and proliferated in three dimensions on the hydrogel scaffold (Fig. 6D). Therefore, the 3D printed hydrogel scaffold is biocompatible for cell culture and has potential to be used as an implant for the replacement of natural elastomers.

Conclusions

In this study, we developed a two-step method for preparing a 3D printable and robust RSF hydrogel. We first used norbornene modified RSF to form a chemically crosslinked network through thiol–ene click reaction. The shear-thinning behaviors of this weak and chemically crosslinked hydrogel are suitable for 3D printing. The subsequent ethanol treatment gives the printed hydrogel high strength and good resilience. The outstanding mechanical properties of this double-network hydrogel are attributed to the constrained growth of β-sheet structures by the chemically crosslinked network. Both networks contribute to form a uniform, dense physically crosslinked network. It should be noted that the compressive and tensile modulus of such a double-network hydrogel reached the same order of magnitude as natural elastomers such as cartilage. Therefore, this two-step method can be a reference for developing other 3D printable hydrogels based on naturally derived polymers with excellent mechanical properties.

Conflicts of interest

There are no conflicts to declare.

Acknowledgements

This work was supported by the National Natural Science Foundation of China (No. 21374020).

References

1 T. Jungst, W. Smolan, K. Schacht, T. Scheibel and J. Groll, Strategies and molecular design criteria for 3D printable hydrogels, *Chem. Rev.*, 2016, **116**, 1496–1539.
2 I. Donderwinkel, J. C. M. V. Hest and N. R. Cameron, Bio-inks for 3D bioprinting: recent advances and future prospects, *Polym. Chem.*, 2017, **8**, 4451–4471.
3 K. Y. Lee and D. J. Mooney, Hydrogels for tissue engineering, *Chem. Rev.*, 2001, **101**(7), 1869–1880.
4 J. B. Costa, J. Silva-Correia, J. M. Oliveira and R. L. Reis, Fast setting silk fibroin bioink for bioprinting of patient-specific memory-shape implants, *Adv. Healthcare Mater.*, 2017, **6**, 1701021.
5 M. K. Wodarczyk-Biegun and A. D. Campo, 3D bioprinting of structural proteins, *Biomaterials*, 2017, **134**, 180–201.
6 M. Hospodiuk, M. Dey, D. Sosnoski and I. T. Ozbolat, The bioink: a comprehensive review on bioprintable materials, *Biotechnol. Adv.*, 2017, **35**(2), 217–239.
7 J. E. Kim, S. H. Kim and Y. Jung, Current status of three-dimensional printing inks for soft tissue regeneration, *Tissue Eng. Regener. Med.*, 2016, **13**(6), 636–646.
8 P. M. Kharkar, K. L. Kiick and A. M. Kloxin, Designing degradable hydrogels for orthogonal control of cell microenvironments, *Chem. Soc. Rev.*, 2013, **42**(17), 7335–7372.
9 J. Y. Li, W. R. K. Illeperuma, Z. G. Suo and J. J. Vlassak, Hybrid hydrogels with extremely high stiffness and toughness, *ACS Macro Lett.*, 2014, **3**(6), 520–523.
10 X. Zhang, Y. H. Yang, J. R. Yao, Z. Z. Shao and X. Chen, Strong collagen hydrogels by oxidized dextran modification, *ACS Sustainable Chem. Eng.*, 2014, **2**(5), 1318–1324.
11 D. H. Su, M. Yao, J. Liu, Y. M. Zhong, X. Chen and Z. Z. Shao, Enhancing mechanical properties of silk fibroin hydrogel through restricting the growth of β-sheet domains, *ACS Appl. Mater. Interfaces*, 2017, **9**, 17489–17498.
12 K. Y. Luo, Y. H. Yang and Z. Z. Shao, Physically crosslinked biocompatible silk-fibroin-based hydrogels with high mechanical performance, *Adv. Funct. Mater.*, 2016, **26**(6), 872–880.
13 E. Desimone, K. Schacht, T. Jungst, J. Groll and T. Scheibel, Biofabrication of 3D constructs: fabrication technologies and spider silk proteins as bioinks, *Pure Appl. Chem.*, 2015, **87**(8), 737–749.
14 S. Xiong, X. Zhang, P. Lu, Y. Wu, Q. Wang, H. Sun, B. C. Heng, V. Bunpetch, S. Zhang and H. Ouyang, A gelatin-sulfonated silk composite scaffold based on 3D printing technology enhances skin regeneration by stimulating epidermal growth and dermal neovascularization, *Sci. Rep.*, 2017, **7**(1), 4288.

15 K. Sun, R. Li, H. Li, D. Li and W. Jiang, Comparison of three-dimensional printing for fabricating silk fibroin blended scaffolds, *Int. J. Polym. Mater. Polym. Biomater.*, 2017, **67**(8), 480–486.

16 H. Lee, G. H. Yang, M. Kim, J. Lee, J. Huh and G. Kim, Fabrication of micro/nanoporous collagen/dECM/silk-fibroin biocomposite scaffolds using a low temperature 3D printing process for bone tissue regeneration, *Mater. Sci. Eng. C*, 2017, **84**, 140–147.

17 N. P. Zhong, T. Dong, Z. C. Chen, Y. W. Guo, Z. Z. Shao and X. Zhao, A novel 3D-printed silk fibroin-based scaffold facilitates tracheal epithelium proliferation in vitro, *J. Biomater. Appl.*, 2019, **34**(1), 3–11.

18 T. Dong, R. X. Mi, M. Wu, N. P. Zhong, X. Zhao, X. Chen and Z. Z. Shao, The regenerated silk fibroin hydrogel with designed architecture bioprinted by its microhydrogel, *J. Mater. Chem. B*, 2019, **7**, 4328–4337.

19 Z. G. Gong, Y. H. Yang, L. Huang, X. Chen and Z. Z. Shao, Formation kinetics and fractal characteristics of regenerated silk fibroin alcogel developed from nanofibrillar network, *Soft Matter*, 2010, **6**(6), 1217–1223.

20 S. Ryu, H. H. Kim, Y. H. Park, C. C. Lin, I. C. Um and C. S. Ki, Dual mode gelation behavior of silk fibroin microgel embedded poly(ethylene glycol) hydrogel, *J. Mater. Chem. B*, 2016, **4**(26), 4574–4584.

21 L. A. Hockaday, K. H. Kang, N. W. Colangelo, P. Y. C. Cheung, B. Duan, E. Malone, J. Wu, L. N. Girardi, L. J. Bonassar, H. Lipson, C. C. Chu and J. T. Butcher, Rapid 3D printing of anatomically accurate and mechanically heterogeneous aortic valve hydrogel scaffolds, *Biofabrication*, 2012, **4**(3), 035005.

22 M. Tsukada, G. Freddi, Y. Gotoh and N. Kasai, Physical and chemical properties of tussah silk fibroin films, *J. Polym. Sci., Part B: Polym. Phys.*, 1994, **32**(8), 1407–1412.

23 B. D. Fairbanks, M. P. Schwartz, A. E. Halevi, C. R. Nuttelman, C. N. Bowman and K. S. Anseth, A versatile synthetic extracellular matrix mimic via thiol-norbornene photopolymerization, *Adv. Mater.*, 2009, **21**(48), 5005–5010.

24 S. Bertlein, G. Brown, K. S. Lim, T. Jungst, T. Boeck, T. Blunk, J. Tessmar, G. J. Hooper, T. B. F. Woodfield and J. Groll, Thiol-ene clickable gelatin: a platform bioink for multiple 3D biofabrication technologies, *Adv. Mater.*, 2017, **29**, 1703404.

25 C. G. Williams, A. N. Malik, T. K. Kim, P. N. Manson and J. H. Elisseeff, Variable cytocompatibility of six lines with photoinitiators used for polymerizing hydrogels and cell encapsulation, *Biomaterials*, 2005, **26**(11), 1211–1218.

26 L. H. Kang, P. A. Armstrong, L. J. Lee, B. Duan, K. H. Kang and J. T. Butcher, Optimizing photo-encapsulation viability of heart valve cell types in 3D printable composite hydrogels, *Ann. Biomed. Eng.*, 2017, **45**(2), 360–377.

27 H. H. Lin, F. Y. Hsieh, C. S. Tseng and S. H. Hsu, Preparation and characterization of biodegradable polyurethane hydrogel and the hybrid gel with soy protein for 3D cell-laden bioprinting, *J. Mater. Chem. B*, 2016, **4**, 6694–6705.

28 P. Monti, P. Taddei, G. Freddi, T. Asakura and M. Tsukada, Raman spectroscopic characterization of Bombyx mori silk fibroin: Raman spectrum of Silk I, *J. Raman Spectrosc.*, 2001, **32**(2), 103–107.

29 P. Monti, G. Freddi, A. Bertoluzza, N. Kasai and M. Tsukada, Raman Spectroscopic Studies of Silk Fibroin from Bombyx Mon, *J. Raman Spectrosc.*, 1998, **29**(4), 297–304.

30 T. Asakura, J. Yao, T. Yamane, K. Umemura and A. S. Ulrich, Heterogeneous structure of silk fibers from Bombyx mori resolved by ^{13}C solid-state NMR spectroscopy, *J. Am. Chem. Soc.*, 2002, **124**(30), 8794–8795.

31 Z. Sui, W. J. King and W. L. Murphy, Protein-based hydrogels with tunable dynamic responses, *Adv. Funct. Mater.*, 2008, **18**(12), 1824–1831.

32 M. A. Tasdelen and Y. Yagci, Light-induced click reactions, *Angew. Chem., Int. Ed.*, 2013, **52**(23), 5930–5938.

